Final Report: Year 3

Nonlinear Aerodynamics and the Design of Wing Tips

Conducted for the
National Aeronautics and Space Administration
Ames Research Center
Grant # NCC2-683

Covering the Period
1 April 1992 to 31 March 1993

by the
Department of Aeronautics and Astronautics
Stanford, California 94305

Principal Investigator
Ilan Kroo

Research Assistant
Sean Wakayama

September 1993

Introduction & Overview

This contract began in April 1990 with studies on the effect of wingtip shape on induced drag. That work considered problems of determining induced drag from computational aerodynamic methods and examined effects of wake roll up on the induced drag of elliptical and crescent wings, [1].

The research contract was continued in April 1991 and again in April 1992 with scope augmented to include considerations other than induced drag. The idea was to develop methods for comparing wing tip shapes on the basis of their effects on total drag, structural weight, and high lift performance. To accomplish this, work was done to improve methods for multidisciplinary analysis and optimization of wings.

This report describes results of research conducted from April 1992 through March 1993. The general objective was to improve an existing wing optimization method, and apply the method to specific problems of interest. The method, while a valuable tool for wing tip design studies, can be applied to more general problems, and has been applied to some of these other problems during its development.

Specific goals that were accomplished are listed below and are explained in more detail in attached reports.

1. Analysis methods were improved in the area of structural modeling.
2. Small improvements to the high lift model were made, and ideas were collected on how clean wing $c_{l_{max}}$ should vary with sweep. These ideas should provide a guide for future examination of high lift with experiment or CFD.
3. A calculation for drag due to the loss of leading edge suction was added to the wing analysis.

Nomenclature

Structural Sizing:

p	Bending stress flow = bending stress times smeared skin thickness.
p_a	Surface pressure.
q	Shear flow.
c_{cs}	Wing box chord.
c_e	Edge chord.
t	Wing thickness.
b_s	Stringer spacing.
L	Rib spacing.
I_{ref}	Dimensionless skin bending inertia.
T_{ref}	Ratio of smeared and actual skin thickness.
z_{cr}	Dimensionless height location of critical stringer stress.
t_s	Skin thickness.
t_{ss}	Smeared skin thickness.
K_s	Local buckling coefficient.
E	Young's modulus.
G	Shear modulus.
σ_y	Yield stress.
ν	Poisson's ratio.
ρ_{mat}	Structural material density.
$I, I_{xx}, I_{xz}, I_{zz}$	Section bending inertias.
J	Section torsional inertia.
A	Area.
A_e	Area enclosed by structural box cross section.
s	Coordinate following perimeter of structural box.
S	Shear.
$\overline{S}$	Effective shear.
q	Dynamic pressure.
q_o	Open section shear flow.
q_c	Constant shear flow for closed sections.
q_t	Total shear flow.
x_{sc}	x location of shear center.
$\vec{U}_\infty$	Freestream velocity vector.
$\hat{U}_\infty$	Unit vector in freestream direction.
$\vec{V}_{ind}$	Induced velocity.
$[AIC]$	Aerodynamic influence coefficient matrix.
$\{bc\}$	Boundary condition vector.
$\hat{n}$	Local panel unit normal vector.
$\bar{\Gamma}$	Vorticity normalized against freestream velocity.
$\text{iconn}(j,i)$	Connectivity function; has value 1 if loads on j affect moments on i; has value 0 otherwise.
$\vec{r}$	Distance vector.
M	Moment.
$[MIC]$	Moment influence coefficient matrix.
w	Wing deflection.
θ	Wing twist due to torsion.
η	Coordinate direction perpendicular to elastic axis of wing.
g	Acceleration of gravity.

m	Mass.
b	Span.
c	Chord.
t	Wing thickness.
t_e	Wing thickness at edge root.
x	Coordinate direction, nominally along freestream.
y	Coordinate direction, nominally pointing to aircraft right.
z	Coordinate direction, nominally pointing up.
δ	Jig twist.
ϕ	Dihedral angle.
Λ	Sweep.
n, n_{lim}	Load factor, limit load factor.
W	Wing weight (mass).
$W_{A/C}$	Aircraft weight.

Leading Edge Suction

Λ	Quarter chord sweep.
Λ_{LE}	Leading edge sweep.
Λ_{TE}	Trailing edge sweep.
c	Chord.
c_n	Normal chord.
c_t	Theoretical thrust coefficient.
t, t_n	Section thickness.
r	Nose radius parameter.
r_n	Nose radius parameter, normal section.
x_{crit}	x/c location of airfoil maximum thickness.
c_{t_n}	Normal thrust coefficient.
c_l	Section lift coefficient.
c_{l_α}	Lift curve slope.
q	Dynamic pressure.
q_n	Dynamic pressure normal to wing.
M	Freestream Mach number.
M	Normal Mach number.
M_e	Effective Mach number.
Re	Reynolds number.
Re_n	Normal Reynolds number.
$c_{p_{lim}}$	Limiting minimum pressure coefficient.
K_t	Leading edge thrust fraction.
i	Section incidence.
i_n	Normal incidence.
c_x, c_z	x and z force coefficients.

Subscripts:

bend	Bending component.
tors	Torsional component.
elastic	Due to wing deformation.
jig	Jig twist value.
ea	Elastic axis.

Wing Weight Estimation

In the area of integrated aerodynamic and structural wing design and optimization, several approaches for evaluating structural weight have been used. One is the statistical wing weight model of which examples are given in references [3] and [4]. Another is a relatively theoretical estimate of bending weight used in references [5] and [6]. A hybrid approach used in reference [7] correlates a theoretical estimate of bending weight to wing weights predicted by a statistical method.

Statistical weight estimates have limited value in planform optimization: since they usually deal with gross properties, they cannot capture the sensitivity of weight to variations in design such as chord extensions and distributions of wing thickness. They are also limited by the range covered by the data used to develop the statistical estimate; results from such estimates have questionable validity when an analyzed design exceeds the existing data.

In estimating actual weights, it is unlikely that a method based upon bending weight would predict actual weights any better than a statistical method. The great difficulty in predicting wing weights is that a large portion of the weight is determined by factors that are impossible or impractical to model accurately at the preliminary design level. Some examples are the weights of access doors and fuel bulkheads. Another problem is actual structures that are overdesigned, for instance in anticipation of growth versions of an aircraft.

In planform optimization, bending weight methods are advantageous because they can better estimate differences in weight due to changes in design. While the B747 has an average t/c of 0.12, the distribution is such that the theoretical root t/c is just under 0.18. While most statistical methods would predict the same weight for wings with the same average t/c, a bending weight method would identify the B747 t/c distribution as more efficient than a wing with uniform t/c, and predict a correspondingly lower weight.

Capturing these differences is important in optimization. If a minimum weight wing is part of the objective, the bending weight method will drive the solution toward a design that is more structurally efficient. In optimization, many of the errors that impede accurate

weight prediction become unimportant. Once a general layout for access doors and bulkheads is determined, the weight of these items is unlikely to change much, so it does not affect the optimal design. If the wing will be overdesigned for growth, then all designs should be heavier by some percentage, so the optimal design will be unchanged.

The bending weight approach may be inadequate because different considerations, such as buckling, may size the structure. This is noticeable when trying to match stiffnesses predicted by a bending weight method to actual stiffnesses. Reference [6] shows that considering static aeroelasticity on aft swept wings at fixed weight will lead to optimal designs with larger spans and less drag. Transitioning between cruise and maneuver, static aeroelasticity causes a relative reduction in the load carried at the wing tips. This reduces bending moments in the maneuver condition, where weight is calculated, while permitting good span efficiencies at cruise, where drag is measured. This presents an advantage over analyzing the wing as though it were rigid, where twisting the wing can be used to reduce bending moments in maneuver, but at the expense of a lower cruise span efficiency. Reference [6] does not attempt to validate its aeroelastic model. In fact, the stiffnesses predicted by that model are somewhat less than actual wing stiffnesses, exaggerating the effect of aeroelasticity. However, the advantages of considering aeroelasticity are great enough to motivate improvements to the bending weight method.

It is possible to incorporate a finite element structural model into wing optimization, as shown in reference [8]. However a simpler model is desirable both for reducing the computer time required for optimization and for limiting the geometric detail necessary to analyze a wing.

For this purpose, a method for predicting structural weight and stiffness was developed. Given information on the shape of the wing box, plus estimates of rib and stringer spacing, the method can predict skin thickness, wing stiffness, and wing weight. The method can also be used to estimate rib and stringer spacings that minimize wing weight.

Approach

Geometry

Wings are modeled with a set of lifting surface elements described by the following parameters: span, area, sweep, dihedral, and taper ratio. To provide the discretization for both aerodynamic and structural models, elements are divided into panels. Twist and thickness to chord ratios are specified at break points. Break points usually lie on element root and tip edges, but may be selected to lie between any two panels in an element. Twist and wing thickness are varied linearly between break points. This scheme provides a concise set of variables for optimization.

The structural model has two levels of detail. The first is used for calculating skin thicknesses and weight. Skin panels are described with skin thickness, t_s, stringer spacing, b_s, and rib spacing, L. The stringer geometry is idealized as scaling with b_s and t_s. This allows the stringer geometry to be represented with three parameters, I_{ref}, z_{cr}, and T_{ref}, as described below.

$$\frac{\text{panel bending inertia}}{\text{unit chordwise length}} = I_{ref} b_s^2 t_s$$

$$\text{height location of maximum stress} = z_{cr} b_s$$

$$T_{ref} = \frac{\text{smeared skin thickness}}{\text{actual skin thickness}}$$

This representation was chosen to facilitate analytic expressions for best rib and stringer spacings that are varied along the span; it does not represent the way a wing would be made. For manufacturing ease, fixed stringer cross sections and spacings are used. Actual stringer designs should be close to optimal in the heaviest sections of a given wing, however, so the weights estimated in the following method should be reasonable.

Ribs are modeled simply as beams running between the wing spars. The rib cross section is modeled as a shear web capped with two booms to take up bending. The web area is A_w; the combined boom area is A_b.

The second level in the structural model treats the wing as a thin walled, single cell monocoque beam and is used to calculate stiffness. The beam cross section has vertical fore and aft spars, parabolic upper and lower skins, and a constant smeared skin thickness around the section. The smeared skin thickness, t_{ss}, combines stringer and spar cap areas with the actual skin thickness, t_s, to obtain an effective thickness for evaluating the bending stiffness.

Structural properties are calculated using methods described in [9]. Bending inertias are calculated in the standard manner.

$$I_{xx} = \int z^2 \, dA; \quad I_{xz} = \int xz \, dA; \quad I_{zz} = \int x^2 \, dA$$

Here x and z are in centroid of area coordinates. Torsional inertias are computed with Bredt-Batho theory.

$$J = \frac{1}{T_{ref}} \frac{4 A_e^2}{\oint \frac{ds}{t_{ss}}}$$

Here A_e is the area enclosed by the shell, ds follows the perimeter of the shell, and t_{ss} is the skin thickness. Division by T_{ref} removes stringer area that is included in the smeared skin thickness but gives little practical contribution to the torsional stiffness.

The x-coordinate of the shear center is calculated by applying positive z shear, S_z, and zero x shear, S_x, in the following equations.

$$\overline{S}_z = \frac{S_z - S_x \frac{I_{xz}}{I_{xx}}}{1 - \frac{I_{xz}^2}{I_{xx} I_{zz}}}$$

$$\overline{S}_x = \frac{S_x - S_z \frac{I_{xz}}{I_{zz}}}{1 - \frac{I_{xz}^2}{I_{xx} I_{zz}}}$$

The above equations evaluate effective shear forces $\overline{S}_x$ and $\overline{S}_z$. The total shear flow in the structure is composed of open and closed components, q_o and q_c.

$$q_t(s) = q_o(s) + q_c$$

The open component is calculated using

$$q_o(s) = -\frac{\overline{S}_z}{I_{xx}} \int_0^s t_{ss} z \, ds - \frac{\overline{S}_x}{I_{zz}} \int_0^s t_{ss} x \, ds$$

The constant term for a closed structure is given by

$$q_c = -\frac{\oint \frac{q_o(s)}{t_{ss}} ds}{\oint \frac{1}{t_{ss}} ds}$$

The x location of the shear center can now be calculated using

$$x_{sc} = -\frac{\oint q_t(s) \, r(s) \, ds}{S_z}$$

Here $r(s)$ is the effective moment arm of the shear flow, $q_t(s)$, to the centroid of area. x_{sc} is the x location of the shear center in centroid of area coordinates.

Aeroelastic Lift Distribution

A method similar to that described in [10] is used to evaluate lift distributions on flexible wings. The wing is represented by a set of discrete horseshoe vortices with bound vortices located at the quarter chord. Vortex strengths are determined by enforcing tangent flow boundary conditions at control points located at three-quarter chord.

$$\vec{U}_\infty \cdot \hat{n}_i + \sum_j \vec{V}_{ind_{ij}} \cdot \hat{n}_i = 0$$

$\hat{n}_i$ is the unit normal vector for panel i. $\vec{V}_{ind_{ij}}$ is the velocity induced at panel i due to the vortex j. It is calculated by integrating velocity contributions over vortex j as per the Biot Savart law. $\vec{V}_{ind_{ij}}$ is proportional to the strength of vortex j yielding the following equation.

$$\sum_j AIC_{ij} \bar{\Gamma}_j = -\hat{U}_\infty \cdot \hat{n}_i$$

or in matrix form

$$[AIC]\{\bar{\Gamma}\} = \{bc\}$$

The aerodynamic influence coefficient matrix, $[AIC]$, relates the vortex strengths to the normal velocities induced at the control points. The boundary condition vector, $\{bc\}$, denotes the flow through the control points due to the freestream. $\bar{\Gamma}$ represents the actual vortex strength normalized by the freestream velocity, U_∞.

Moments, needed to calculate elastic deformations and size skin thicknesses, are evaluated to first order by

$$\vec{M}_i = \sum_j 2q \ \text{iconn}(j,i) \left(\vec{r}_{ij} \times (\hat{U}_\infty \times \vec{G}) \right) \bar{\Gamma}_j$$

The vector $\vec{r}_{ij}$ points from the shear center of panel i to the bound vortex center of panel j. The function, $\text{iconn}(j,i)$, has value one when loads on j logically affect moments on i; it has value zero when loads on j have no influence, as when panel j lies inboard of panel i. The vector, $\vec{G}$, runs from root to tip of bound vortex j.

The moment vector is separated into bending and torsional components about the elastic axis.

$$\{M_{bend}\} = q\,[MIC_{bend}]\{\bar{\Gamma}\}$$
$$\{M_{tors}\} = q\,[MIC_{tors}]\{\bar{\Gamma}\}$$

Integrating these moments along the span yields elastic slope and twist deformations.

$$\frac{dw}{d\eta} = \int \frac{M_{bend}}{EI} d\eta; \quad \theta = \int \frac{M_{tors}}{GJ} d\eta$$

These deformations are related, through coordinate transformations, to changes in panel incidences, as indicated by the following equations for panel unit normal vector.

$$\begin{aligned}
n_x &= \sin\delta + \theta \cos\Lambda_{ea} \cos\delta - \tfrac{dw}{d\eta} \sin\Lambda_{ea} \cos\delta \\
n_y &= -\sin\phi\cos\delta \\
&\quad - \theta(\cos\phi \sin\Lambda_{ea} \cos\delta - \sin\phi \cos\Lambda_{ea} \sin\delta) \\
&\quad - \tfrac{dw}{d\eta}(\cos\phi \cos\Lambda_{ea} \cos\delta + \sin\phi \sin\Lambda_{ea} \sin\delta) \\
n_z &= \cos\phi\cos\delta \\
&\quad - \theta(\sin\phi \sin\Lambda_{ea} \cos\delta + \cos\phi \cos\Lambda_{ea} \sin\delta) \\
&\quad - \tfrac{dw}{d\eta}(\sin\phi \cos\Lambda_{ea} \cos\delta - \cos\phi \sin\Lambda_{ea} \sin\delta)
\end{aligned}$$

Through the integration and transformations above, $\hat{n}$ is linearly related to the vortex strengths. Recalling that $\{bc\} = \hat{U}_\infty \cdot \hat{n}$, we see that

$$\{bc\} = \{bc_{jig}\} + \{\Delta bc_{elastic}\}$$

where

$$\Delta bc_{elastic} = qK_{bend_i} \sum_j \frac{\text{iconn}(i,j)}{EI_j} \sum_k MIC_{bend_{jk}} \bar{\Gamma}_k + qK_{tors_i} \sum_j \frac{\text{iconn}(i,j)}{GJ_j} \sum_k MIC_{tors_{jk}} \bar{\Gamma}_k$$

or

$$\{\Delta bc_{elastic}\} = -[SIC]\{\bar{\Gamma}\}$$

Recalling the relationship $[AIC]\{\bar{\Gamma}\} = \{bc\}$, the equation for determining the vorticity distribution with aeroelastic deformation is then

$$[AIC]\{\bar{\Gamma}\} + [SIC]\{\bar{\Gamma}\} = \{bc_{jig}\}$$

Refinement to Aeroelastic Loads

While developing the method for obtaining wing weight, it was found that zero lift pitching moment and inertial bending relief had small but noticeable effects when estimating wing weights of existing transports. These effects are modeled by altering the boundary condition vector.

Moments from zero lift pitching moments are calculated using

$$\vec{M}_{0_i} = \sum_j q \cos^2 \Lambda \; c_{m_{0_j}} c_j^2 \; \text{iconn}(j,i)(G_{y_j}\hat{y} + G_{z_j}\hat{z})$$

The $\cos^2 \Lambda$ accounts for simple sweep effects. G_y and G_z express y and z components of the panel width.

Inertial bending relief is handled simply.

$$\vec{M}_{M_i} = \sum_j -ngm_j\vec{r}_{m_{ij}} \times \hat{z}$$

Here g is the acceleration of gravity, n is the load factor, m_j is the mass at panel j, and $\vec{r}_{m_{ij}}$ is the vector from shear center of panel i to the shear center of panel j. The panel mass, m_j, includes mass of the wing structure, fuel contained in the wing, and any engines mounted at the panel. Fuel mass is estimated using

$$m_{fuel} = FF\rho_{fuel}A_e\frac{\Delta b}{\cos\Lambda_{ea}}$$

Here A_e is the cross sectional area of the structural box in the plane perpendicular to the shear center sweep. $\Delta b/\cos\Lambda_{ea}$ is the panel width in structural coordinates. ρ_{fuel} is the density of the fuel and FF is the fraction of available volume occupied by fuel.

Load Cases

Structural weight is evaluated using as many as six loading conditions. All flight loading conditions are evaluated at a specified structural design altitude and Mach number. Four of these are done at maximum weight with zero wing fuel: cruise, maneuver, vertical and lateral gust. A separate maneuver condition is evaluated for the aircraft at maximum takeoff weight with full wing fuel. Maneuver load factor and gust velocities are specified. A gust alleviation factor is applied to vertical gust velocities. The final loading condition is a taxi bump in which the wing, with full wing fuel, must sustain a 1.5 g vertical acceleration.

The maneuver condition with full wing fuel is often critical. Although the wing receives bending relief from the fuel inertia, the fuel is normally distributed close to the wing root, making the inertia relief less than the bending moments due to the extra load. The gust conditions are evaluated at zero fuel weight because, to first order, the total load generated by a gust is constant regardless of the aircraft weight. The zero wing fuel case is then critical because of the lack of bending relief. The taxi bump was added when the optimizer began to create wing tip tanks to maximize inertia relief. In ground handling, without counteracting air loads, the weight of tip tanks can generate moments in excess of the flight loads, and the taxi condition is used to properly penalize such designs.

Structural Design Constraints

To estimate the weight and stiffness of the wing box, eight constraints on the design of the wing structure are considered.

The first constraint is that the skin should not yield under a specified pressure load, p_a. For bending of the skin between stringers this constraint requires

$$t_s \geq \sqrt{\frac{3p_a b_s^2}{4\sigma_y}}K_1 \qquad (1)$$

Under the same specified pressure, the skin-stringer panels supported between ribs must also not yield.

$$t_s \geq \frac{p_a L^2 z_{cr}}{8I_{ref}b_s^2\sigma_y}K_2 \qquad (2)$$

Stress loads from wing bending are considered next. The fully stressed criteria requires

$$t_s \geq \frac{p}{\sigma_y T_{ref}}K_3 \qquad (3)$$

Since these stresses are in the same direction as those for panel bending, the two preceding constraints are combined as follows:

$$t_s \geq \frac{p_a L^2 z_{cr}}{8I_{ref}b_s^2\sigma_y}K_2 + \frac{p}{\sigma_y T_{ref}}K_3 \qquad (2a)$$

Buckling of the skin between stringers is handled in a local buckling constraint.

$$t_s \geq \left[\frac{12(1-\nu^2)pb_s^2}{\pi^2 K_s E}\right]^{\frac{1}{3}}K_4 \qquad (4)$$

The buckling of skin-stringer panels between ribs is also considered.

$$t_s \geq \frac{pL^2}{\pi^2 E I_{ref} b_s^2} K_5 \tag{5}$$

The first constraint affecting sizing of the ribs is the requirement to carry the specified pressure loads to the wing spars. The shear web sized by this requirement has area

$$A_w \geq \frac{\sqrt{3} p_a c_{cs} L}{2\sigma_y} K_6 \tag{6}$$

The required boom area to support bending stresses is

$$A_b \geq \frac{p_a c_{cs}^2 L}{4\sigma_y t} K_7 \tag{7}$$

The final design constraint is the rib stiffness required to force panel buckling to occur in cells dictated by the rib spacing and not in lower energy modes involving deflection of the ribs. The boom area to do this is given by

$$A_b \geq \frac{5pc_{cs}^4}{48Et^2L} K_8 \tag{8}$$

Estimates for Minimum Weight Geometry

Using the given constraint equations, it is possible to analytically determine a geometry that will minimize the weight of the skin, stringer, and rib structure. The procedure is to pick sets of constraints that will be active, describe rib and stringer spacings as constrained functions of the skin thickness, express the structural weight per unit area as a function only of the skin thickness, and derive an expression for the skin thickness minimizing W/S. To simplify matters, we can neglect constraints 2, 3, 6, and 7. Constraint 2a will become critical before constraints 2 and 3. Constraints 6 and 7 do not vary with skin thickness or rib or panel spacings.

To size the structure, optimal skin thicknesses are evaluated for four possible combinations of constraints plus minimum gauge. The largest skin thickness is taken to be critical and is applied to the constraint equations to determine b_s and L. Equations for the four constraint combinations are given below.

Skin sizing for the case where constraints 4, 5, and 8 are active:

$$b_s^2 = \frac{\pi^2 K_s E}{12(1-\nu^2)p} \frac{t_s^3}{K_4^3}$$

$$L^2 = \frac{\pi^4 K_s E I_{ref}}{12(1-\nu^2)p^2} \frac{t_s^4}{K_4^3 K_5}$$

$$\frac{(W/S)}{\rho_{mat}} = 2T_{ref} t_s + \frac{5(1-\nu^2)p^3 c_{cs}^4 K_4^3 K_5 K_8}{4\pi^4 K_s E^2 I_{ref} t^2 t_s^4} + \frac{A_w}{L}$$

$$t_s^5 = \frac{5(1-\nu^2)p^3 c_{cs}^4 K_4^3 K_5 K_8}{2\pi^4 K_s E^2 I_{ref} T_{ref} t^2}$$

When constraint 2a is active, the sizing algorithm is more complicated. We define two variables,

$$t_{s_2} = \frac{p_a L^2 z_{cr}}{8 I_{ref} b_s^2 \sigma_y} K_2$$

$$t_{s_3} = \frac{p}{\sigma_y T_{ref}} K_3$$

The required skin thickness is

$$t_s = t_{s_2} + t_{s_3}$$

The equations for sizing the skin structure when constraints 2a, 4, and 8 are active are

$$b_s^2 = \frac{\pi^2 K_s E}{12(1-\nu^2)p} \frac{(t_{s_2}+t_{s_3})^3}{K_4^3}$$

$$L^2 = \frac{8 I_{ref} \sigma_y}{p_a z_{cr}} b_s \frac{t_{s_2}}{K_2}$$

$$\frac{(W/S)}{\rho_{mat}} = 2T_{ref}\left[(t_{s_2}+t_{s_3}) + \frac{T}{(t_{s_2}+t_{s_3})^{\frac{3}{2}} t_{s_2}}\right] + \frac{A_w}{L}$$

where

$$T = \frac{5pp_a c_{cs}^4 z_{cr} K_2 K_8}{192 E I_{ref} \sigma_y t^2 (2T_{ref})} \sqrt{\frac{3(1-\nu^2)pK_4^3}{\pi K_s E}}$$

Minimizing with respect to t_{s_2} yields the following equation that can be quickly solved using Newton's method on the range $t_{s_2} > 0$.

$$(t_{s_2}+t_{s_3})^{\frac{5}{2}} t_{s_2}^2 - T(\frac{5}{2} t_{s_2} + t_{s_3}) = 0$$

Skin sizing for the case where constraints 1, 5, and 8 are active:

$$b_s^2 = \frac{4\sigma_y}{3p_a} \frac{t_s^2}{K_1^2}$$

$$L^2 = \frac{\pi^2 E I_{ref}}{p} b_s \frac{t_s}{K_5}$$

$$\frac{(W/S)}{\rho_{mat}} = 2T_{ref} t_s + \frac{5p^2 p_a c_{cs}^4 K_1^2 K_5^2 K_8}{64\pi^2 E^2 I_{ref} \sigma_y t^2 t_s^3} + \frac{A_w}{L}$$

$$t_s^4 = \frac{15p^2 p_a c_{cs}^4 K_1^2 K_5^2 K_8}{128\pi^2 E^2 I_{ref} T_{ref} \sigma_y t^2}$$

Skin sizing for the case where constraints 1, 2, and 8 are active:

$$b_s^2 = \frac{4\sigma_y}{3p_a} \frac{t_s^2}{K_1^2}$$

$$L^2 = \frac{8 I_{ref} \sigma_y}{p_a z_{cr}} b_s \frac{t_s}{K_2}$$

$$\frac{(W/S)}{\rho_{mat}} = 2T_{ref} t_s + \frac{5\pi^2 p_a^3 z_{cr}^2 c_{cs}^4 K_1^2 K_2^2 K_8}{4096 I_{ref} \sigma_y^3 t^2 t_s^3} + \frac{A_w}{L}$$

$$t_s^4 = \frac{15\pi^2 p_a^3 z_{cr}^2 c_{cs}^4 K_1^2 K_2^2 K_8}{8192\pi^2 E^2 I_{ref} T_{ref} \sigma_y^3 t^2}$$

The above expression was developed before constraint 2a was conceived. The more complicated expression for the case where constraints 1, 2a, and 8 are active has not been developed since we have not found a case where constraint 1 was critical before constraint 3.

Estimates for Leading and Trailing Edge Weight

Leading and trailing edges can be sized in a manner similar to the main box. These structures transmit pressure loads into the wing box and are too light to carry wing bending loads. The active constraints are 1, 6, and 7. They require slight modification to account for the different geometry.

$$t_s \geq \sqrt{\frac{3p_a L^2}{4\sigma_y}} K_1 \tag{1}$$

$$A_w \geq \frac{\sqrt{3} p_a c_e L}{\sigma_y} K_6 \tag{6}$$

$$A_b \geq \frac{p_a c_e^2 L}{\sigma_y t_e} K_7 \tag{7}$$

There is not much to optimize here. Rib (W/S) is not dependent on L. Skin (W/S) suggests L goes to zero. The structure is then sized by minimum gauge with L just large enough to make constraint 1 critical.

Weight Prediction Details

Up to now, we have only outlined the theoretical model for the weight prediction method. We now must translate these into actual weight estimates.

Material properties are taken as follows: $E = 72.4$ GPa, $G = 27.6$ GPa, $\nu = 0.34$, $\sigma_y = 345$ MPa.

While wing bending moments are calculated to get bending flow, p, directly, the design skin pressure, p_a, is a parameter that needs to be provided. In the wing box, this pressure affects the sizing of stringers by adding stress in same direction as the wing bending stress. This pressure is estimated using average lift pressures on a flat plat airfoil. The critical average lift pressure on the wing is $(W_{A/C}/S)n_{lim}$. The chordwise distribution is skewed toward the nose, so over the wing box, the pressures are somewhat lower. The following formula is used:

$$p_a = 0.83(W_{A/C}/S)n_{lim}SF$$

The factor 0.83 accounts for the average lift pressure between 0.175 and 0.625 chord on a flat plate airfoil, representative of the chordwise extent of the wing box on transport aircraft. This is conservative in the sense that all the lift is assumed to be generated on one surface. Compensating for this are the effects of thickness, which would increase pressure differences.

An alternate approach to estimating design skin pressure is to take $p_a = qc_pSF$. This would require knowing c_p distribution on representative wing sections at the critical load condition.

The maximum pressures experienced on leading edges are higher, so the following formula is used.

$$p_a = 2.95(W_{A/C}/S)n_{lim}SF$$

The factor 2.95 accounts for the average lift pressure between the leading edge and 0.175 chord on a flat plate airfoil.

Trailing edges, in which we include flap and aileron structure, are sized by limiting flap or aileron loads. These are often experienced at a condition other than the limit maneuver or gust load. In the case of flaps, the critical condition is probably at maximum flaps extended speed. Assuming this speed is set at similar C_L on different aircraft, the dynamic pressure setting the flap structural design will vary like aircraft wing loading. Assuming flaps will provide similar increments to section c_l, the flap pressures should also vary with wing loading. As flaps are the largest component of our defined trailing edge weight, the following formula is used to set the design trailing edge pressure.

$$p_a = 3.0(W_{A/C}/S)SF$$

The factor 3.0 is based upon a flap normal load limit of 322 lb/ft^2 on the DC9-32 with MTOW = 108000 lb, [11].

To evaluate weights, the following formulas are used. For the weight of skin, spars, and stringers in the wing box

$$W_{skin} = \int \rho_{mat} P_s T_{ref} t_s \, db$$

Here, P_s is the box perimeter and db is the incremental span. The weight of ribs in the wing box is calculated using

$$W_{rib} = \int \rho_{mat} \frac{A_w + A_b}{L} c_{cs} \, db$$

The weight of leading or trailing edges is calculated using

$$W_{edge} = K_{edge} \int \rho_{mat} \left(2T_{ref} t_s + \frac{A_w + A_b}{L} \right) c_e \, db$$

Here, K_{edge} is a constant correction factor, converting our idealized weight to an estimate of actual weight.

There is a considerable amount of weight that we cannot evaluate without a more detailed model and information on actual loads. These include the weight of joints, doors, wing fuselage attachment, fuel boundaries, landing gear support, fairings, and fillets. We assume this weight to be proportional to the maximum wing loading.

$$\frac{W_{other}}{S} = K_{other}(W_{A/C}/S)n_{lim}/g$$

For this study, $K_{other} = 9.09 \times 10^{-3}$, based upon a fit to weight unaccounted for by other weight categories.

For this weight study, the following dimensionless stringer geometry was used: $I_{ref} = 1.40325 \times 10^{-2}$, $T_{ref} = 1.69$, $z_{cr} = 0.25740$, $K_s = 5.236$. These numbers apply roughly to a Z-stringer design with stringer height 0.3 times the stringer spacing, flange width 0.09 times the stringer spacing, and stringer thickness equal to the skin thickness. The buckling parameter was obtained from reference [12].

The following correction constants were used. $K_1 = K_2 = K_3 = K_4 = K_5 = K_6 = 1$, no correction for non optimal skin or stringer material. $K_7 = K_8 = 3$, equivalent to spreading the area concentrated in the rib booms evenly over the height of the rib web. To account for extra joint or non optimal weight, correction factors are applied to leading and trailing edge weights. In the case of trailing edges, the correction also accounts for the weight of supports for the flaps and ailerons. The corrections used were based upon a fit with actual weights, $K_{LE} = 1.6$ and $K_{TE} = 2.7$.

Results

The resulting wing weight estimates are compared against data from Douglas and Boeing estimates and weight statements in table 2.

A few comments on the weight results are in order. Rib weight is not intended to cover the actual weight of ribs, only the weight necessary to support the skin against buckling or panel bending. The weight of ribs serving to transmit flap, aileron, engine, landing gear, and side of body loads are absorbed into the other weight category as is the weight of bulkheads.

It was decided not to include leading edge device weight in leading edge weight because of a large variation in the actual weight of such devices: a factor of two between the DC9 and B737. The weight due to a leading edge slot on the DC8 could not be separated out, so the difference between computed and actual leading edge weights for that aircraft is large. The weight of leading edge devices is absorbed into other weight. Note that the Citation has no leading edge device and if this were taken into account, the weight estimate would be improved.

The method yields reasonable stiffness estimates when applied to commercial aircraft. Figures 1 and 2 compare stiffness estimates from the method with manufacturer's estimates for a particular transport. Reasonable agreement is found near the root. In the tip region, the method underestimates wing stiffness by predicting rib and stringer spacings that are too small. With smaller rib and stringer spacings, buckling and panel bending constraints are eased making it possible to tolerate higher stresses and use thinner skins. The consideration that would call for larger rib spacing is the rib weight required to stabilize the skin panels in

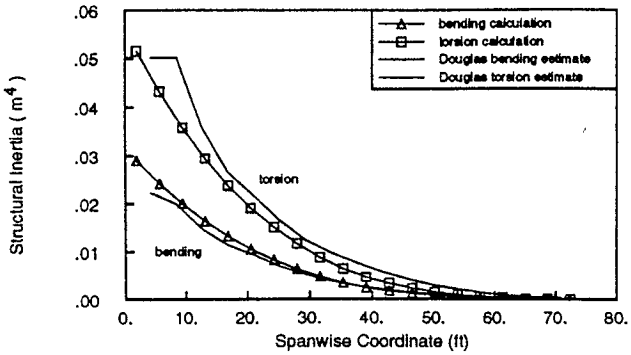

Figure 1: Wing stiffnesses calculated through the optimal skin sizing routine as compared to actual stiffnesses.

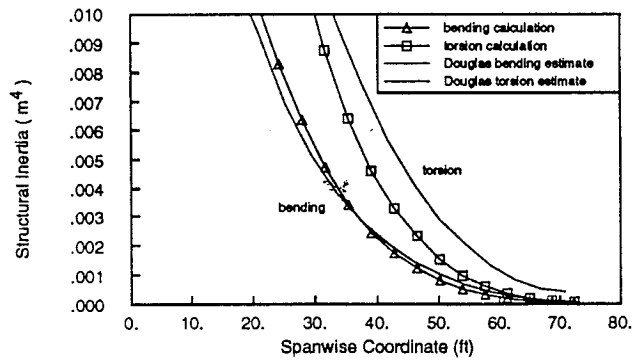

Figure 2: Wing stiffnesses calculated through the optimal skin sizing routine as compared to actual stiffnesses. Enlarged to show detail at the wing tips.

		DC9-32	DC8-55	B737-200	B747-200	Citation
Area		1001	2883	1005	5469	269
Span		93.31	142.40	93.00	195.67	43.92
Planform Break % Span		30	55	35	40	
Chord	Root	17.80	32.71	21.92	51.37	8.79
	Break			10.69	27.45	
	Tip	3.63	7.52	4.82	12.67	3.43
Dihedral		2.5 6.5	6.0	6.0	4.0	
Sweep	Inboard	24.5	30.6	28.0	37.5	1.4
	Outboard	24.5	30.6	25.0	37.5	1.4
t/c	Root	0.1310	0.1260	0.1264	0.1794	0.1400
	Break	0.1090	0.0950	0.1082	0.0789	
	Tip	0.0830	0.0970	0.1122	0.0777	0.1200
Spar x/c	Front	0.193	0.175	0.175	0.175	0.300
	Rear	0.606	0.625	0.625	0.625	0.625
Incidence (% Span)		0.00 (0)	0.00 (0)	0.00 (0)	0.00 (0)	0.00 (0)
		-0.20 (30)	-0.20 (30)	0.35 (35)	0.35 (40)	
		-1.39 (70)	-1.39 (70)	1.24 (75)	1.24 (70)	
		-3.04 (100)	-3.04 (100)	2.02 (100)	2.02 (100)	-3.00 (100)
Engine Weight (% Span)	Inboard		6977 (37.5)	4511 (32.5)	9437 (37.5)	
	Outboard		7210 (62.5)		9437 (67.5)	
MTOW		108000	325000	115500	708000	11500
MZFW		87000	224000	95000	526500	8900
Fuel Weight	23678	148289	24364	308962	3500	

Table 1: Wing definition for the sample aircraft. This is the data used to evaluate wing weights for comparison with actual weights. Many entries are estimates because actual data was not available. Units are applied as follows: weights in pounds, lengths in feet, angles in degrees.

		DC9-32	DC8-55	B737-200	B747-200	Citation
Skin & Spar Weight	Calculated	3411	12123	4541	47124	317
	Actual	4607	14789	5432	48513	
	Ratio	0.74	0.82	0.84	0.97	
Rib Weight	Calculated	275	2276	357	3963	13
Leading Edge Weight	Calculated	558	1668	499	3592	222
	Actual	464	2556	402	4000	
	Ratio	1.20	0.65	1.24	0.90	
Trailing Edge Weight	Calculated	2182	7435	2092	16543	404
	Actual	1979	6525	2606	17957	
	Ratio	1.10	1.14	0.80	0.92	
Other Weight	Calculated	2455	7387	2625	16091	520
Total Weight	Calculated	8881	30889	10114	87314	1475
	Actual	11394	34909	10775	88202	1020
	Ratio	0.78	0.88	0.94	0.99	1.45

Table 2: Wing weight estimates as compared with Douglas and Boeing estimates and weight statements. Weights are given for the complete wing in pounds.

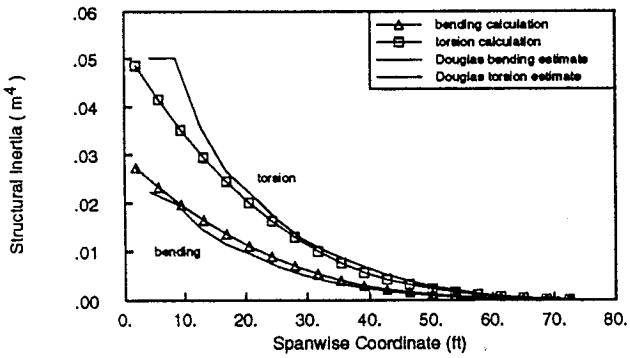

Figure 3: Wing stiffnesses calculated using fixed rib and stringer spacings as compared to actual stiffnesses.

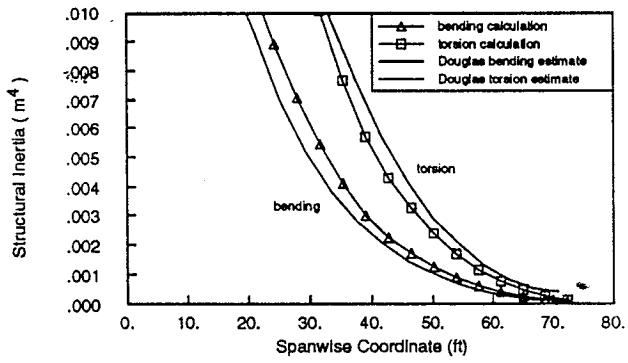

Figure 4: Wing stiffnesses calculated using fixed rib and stringer spacings as compared to actual stiffnesses. Enlarged to show detail at the wing tips.

panel buckling. Since bending loads are small near the tip, the required rib weight is also small, making increases in rib weight due to closer rib spacings less than the corresponding decreases in skin weight.

A better estimate of wing stiffness can be obtained if

rib and stringer spacings are fixed to match the spacings on the actual aircraft. Figures 3 and 4 show stiffnesses calculated assuming a uniform stringer spacing of 6 inches and a uniform rib spacing of 2 feet. Torsional stiffness is underpredicted because of differences between the assumed and actual stringer geometries, particularly in the estimated value of T_{ref}.

Although better stiffness estimates can be obtained when the rib and stringer layout is known, using the optimal structural layout method provides other valuable information including an estimate of minimum possible structural weight and an estimate for what the structural layout should be if it is not known. A reason for developing the optimal structural layout method was to have a method applicable to a wide range of aircraft. This method automatically reduces rib and stringer spacings for small aircraft, where using spacings for commercial aircraft would lead to more overprediction of wing weight. A weakness of the method in this respect is that it cannot optimize details of the stringer design. For instance, on the B747, the ratio of skin plus stringer weight to skin weight is significantly larger than the 1.69 used in this study. The heavier stringer design could give a lower wing weight by increasing I_{ref} thereby reducing the skin thickness required to meet the panel bending constraint.

Conclusions

A method for estimating wing weight and stiffness has been developed. This method accounts for many constraints affecting the structural design of a wing, including bending stresses, buckling, and support of local pressure loads. The method can provide reasonable weight and stiffness estimates.

While the method gives better stiffness estimates when given information on actual rib and stringer spacings, it can also estimate best layouts for minimum weight giving it potential to be applied over a wide range of aircraft sizes. By covering a large set of constraints and having some flexibility in tuning the detailed structural design, it is hoped that this method will capture the critical constraints that affect the weight of a wing. If successful, this method can be a useful structural model for wing optimization programs.

Thoughts on Maximum Lift Predicition

This section attempts to provide explanations for the simple high lift model used in the Wing Aerodynamics and Structures Program.

Clean Wing

Most all preliminary design methods for predicting maximum lift begin with clean wing maximum lift and add increments due to flaps and leading edge devices. WASP uses a critical section approach, declaring the wing at its maximum useful lift when any section gets within a certain tolerance of its $c_{l_{max}}$.

This approach is straightforward for unswept wings. For swept wings a major problem is determining a section $c_{l_{max}}$ to use with the critical section approach. Simple sweep theory suggests that $c_{l_{max}}$ varies with $\cos^2 \Lambda$. According to experiments, this is much too conservative, [13].

There are two reasons for this. First, leading edge separation can result in a vortex flow where low pressures from the vortex act upon the upper surface of the wing and actually create lift. In extreme cases, this can result in $c_{l_{max}}$ that increases with sweep. Second, the boundary layer flow follows the freestream direction more than the sweep normal direction and this extra freedom delays the loss of lift.

To deal with leading edge vortex flow, the leading edge suction method of Carlson, Mack, and Barger is used, [18]. This predicts changes in lift and drag due to the loss of leading edge suction and the formation of a leading edge vortex.

On sections without leading edge vortex flow, we need to decide upon a rational choice for the variation of $c_{l_{max}}$ with sweep. There is much evidence supporting that $c_{l_{max}}$ varies with $\cos \Lambda$. An argument supporting this can be fashioned from simple sweep and thin airfoil theory.

The argument begins with the following motivational problem: given t/c and camber for a section on a swept wing, determine the 2D section that gives the closest matching pressure distribution. If the pressure distributions match, then similar boundary layer flows are likely.

We assume an airfoil geometry defined in the freestream direction.

$$z(x) = z_c(x) \pm z_t(x)$$

We allow the geometry to be scaled.

$$z(x) = z_{ref} \left(\zeta_c(x) \pm \zeta_t(x)\right)$$

If we apply thin airfoil theory, we get a velocity distribution that is a function of the geometry.

$$\frac{U}{U_\infty} = 1 + z_{ref}\mu_t(x) \pm (\alpha\mu_\alpha(x) + z_{ref}\mu_c(x))$$

Where $\mu(x)$ are perturbation velocities per unit t/c, α, or camber, as functions of the ζ geometry functions.

We use simple sweep theory to obtain freestream pressure coefficients.

$$
\begin{aligned}
c_p &= \frac{p - p_\infty}{\frac{1}{2}\rho Q_\infty^2} \\
&= -2\left(\frac{q}{Q_\infty}\right) - \left(\frac{q}{Q_\infty}\right)^2 \\
&= \left[-2\left(\frac{u}{U_\infty}\right) - \left(\frac{u}{U_\infty}\right)^2\right]\cos^2\Lambda \\
&= -2\left[z_{ref_\perp}\mu_t \pm \left(\alpha_\perp \mu_\alpha + z_{ref_\perp}\mu_c\right)\right]\cos^2\Lambda - \\
&\quad \left[z_{ref_\perp}\mu_t \pm \left(\alpha_\perp \mu_\alpha + z_{ref_\perp}\mu_c\right)\right]^2 \cos^2\Lambda
\end{aligned}
$$

Where

$$\alpha_\perp = \frac{\alpha}{\cos\Lambda}, \quad \text{and} \quad z_{ref_\perp} = \frac{z_{ref}}{\cos\Lambda}$$

This can be rewritten in terms of the freestream geometry.

$$
\begin{aligned}
&= -2\left[z_{ref}\mu_t \pm \left(\alpha\mu_\alpha + z_{ref}\mu_c\right)\right]\cos\Lambda - \\
&\quad \left[z_{ref}\mu_t \pm \left(\alpha\mu_\alpha + z_{ref}\mu_c\right)\right]^2
\end{aligned}
$$

In the last equation, the $\cos\Lambda$ term is dominant in determining lift. The velocity squared term determines the peak pressure. If peak pressures are matched to those on an unswept wing with the same freestream section, then the lift will be reduced by $\cos\Lambda$.

In predicting maximum lift, matching peak pressures is significant because it can give an indication of separation on the forward part of the airfoil, where pressures are lowest. Since the boundary layer flow is sensitive to pressure and pressure gradient, and it is insensitive to the downstream flow, separation near the leading edge of a swept wing might be predicted by matching the pressure distribution near that leading edge with a pressure distribution known to cause separation on a 2D section.

The rationale for saying $c_{l_{max}}$ varies with $\cos\Lambda$ then goes as follows. When a swept section approaches $c_l = c_{l_{max}}|_{\Lambda=0}\cos\Lambda$, the pressure distribution at the nose approaches that of the same section at unswept $c_{l_{max}}$. As this pressure distribution is known to give massive separation in the unswept case, we also expect stall in the swept case. Figures 5 and 6 illustrate how peak pressures are matched.

An exception to predicting stall according to leading edge separation occurs with leading edge vortex flow. To deal with this, the program checks for $c_{l_{max}}$ violations before calculating lift due to any leading edge vortices. That is, lift due to leading edge vortex flow is included as an increment to a calculated clean wing $C_{L_{max}}$. There is certainly a question whether this is correct, but most wings are operated with slats extended in the high lift region, meaning we would not normally worry about this leading edge vortex flow.

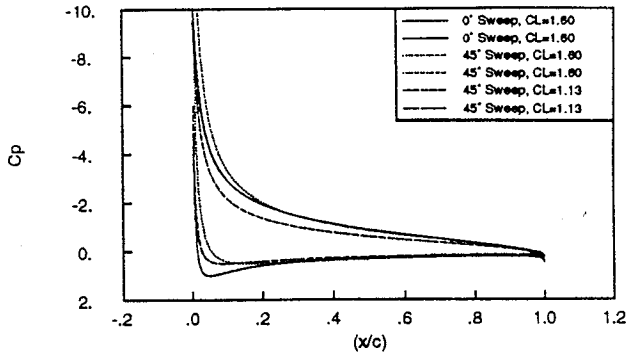

Figure 5: Pressure distributions for unswept and infinite span swept wings. Wings have NACA 0012 section perpendicular to the sweep direction. Calculation through simple sweep theory and thin airfoil theory with Reigel's correction. Pressure coefficients are referenced against freestream velocity. When lift coefficients are matched, peak pressures on the swept wing are greater, but pressures over the major portion of the section are the same. When swept wing lift coefficient is set to the unswept wing lift coefficient reduced by $\cos\Lambda$, peak pressures on the swept wing are close to those on the unswept wing.

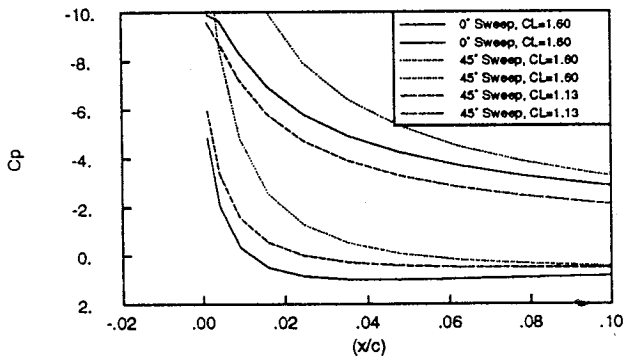

Figure 6: Pressure distributions for unswept and infinite span swept wings. Same as figure 1, but with emphasis on the peak pressures near the leading edge.

The arguments presented above are not rigorous and they require substantiation by experiments or analysis on problems using codes capable of predicting separation. At present, it is hoped to run a Navier Stokes code on a series of swept wings to determine how accurate the above arguments are.

Slats

The increment in $c_{l_{max}}$ due to slats is taken from data presented by Callaghan, [15], that shows a variation like $\cos^n \Lambda$, with n between 2 and 3. The implementation in the code takes a variation with $\cos^2 \Lambda$. It is important that different increments to $c_{l_{max}}$ do not overlap. In using Callaghan's increment due to slats, there is an implicit assumption that his increment was measured for sections that did not have leading edge vortex flow, and that increments to $c_{l_{max}}$ due to this flow are not imbedded in Callaghan's measurements.

The increment in drag coefficient due to slats is taken as .006 from Shevell, [16].

Flaps

Flaps should follow the $\cos \Lambda$ rule as with clean sections. Flaps work by increasing the lift carried over the rear of the airfoil. This increases the total lift available when loads at the nose lead to separation. Considering only inviscid flow about a wing with given flap deflection, measured about an axis perpendicular to the freestream flow, the lift due to the flap diminishes with $\cos \Lambda$. (In simple sweep theory the normal q is reduced by $\cos^2 \Lambda$, but the normal flap deflection is increased by $\frac{1}{\cos \Lambda}$.) By working the rear of the airfoil harder, flaps increase c_l at a given angle of attack and retain a fraction of that c_l increment at $c_{l_{max}}$. The increment to $c_{l_{max}}$ due to flaps is mostly proportional to the increment in c_l, [17]. On swept wings, since the increment in c_l varies with $\cos \Lambda$ we expect the increment in $c_{l_{max}}$ to also vary with $\cos \Lambda$.

Implementation of Leading Edge Suction Calculation

The method for calculating loss of leading edge suction in the wing analysis program follows closely the method given a report by Carlson, Mack, and Barger, [18]. Leading edge normal Mach number is calculated through

$$M_n = M \cos \Lambda_{LE}$$

Theoretical leading edge thrust coefficient is calculated through

$$c_t = \frac{c_l (c_l - c_{l_0}) \sqrt{1 - M_n^2}}{2\pi \cos \Lambda}$$

The above expression is equivalent to

$$c_t = c_l \alpha$$

with

$$c_{l_\alpha} = \frac{2\pi \cos \Lambda}{\sqrt{1 - M_n^2}}$$

and c_{l_0} representing the lift coefficient at zero angle of attack.

It is possible for c_t to be less than zero if the airfoil generates positive lift at negative angle of attack. The thrust coefficient is negative because of high pressure caused by stagnation on the nose. In this condition it is likely that leading edge suction will be retained. In the programming implementation, a negative c_t will cause problems, such as square roots of negative numbers. Because of this, if a negative c_t is encountered, the algorithm simply assumes that full leading edge suction is retained.

At this point the algorithm follows the method of reference [18] exactly until the leading edge thrust factor is obtained.

$$c_n = \frac{2 x_{crit} c}{\sin \Lambda_{LE} \left[(1 - x_{crit}) \tan \Lambda_{LE} + x_{crit} \tan \Lambda_{TE} \right] + \cos \Lambda_{LE}}$$

$$\frac{t_n}{c_n} = \frac{t}{c} \frac{1}{2 x_{crit} \cos \Lambda_{LE}}$$

$$\frac{r_n}{c_n} = \frac{r}{c} \frac{1}{2 x_{crit} \cos^2 \Lambda_{LE}}$$

$$Re_n = Re\, c_n \cos \Lambda_{LE}$$

$$c_{p_{lim}} = \frac{-2}{\gamma M_n^2} \left[\frac{Re_n \times 10^{-6}}{Re_n \times 10^{-6} + 10^{(4 - 3M_n)}} \right]^{0.05 + 0.35(1 - M_n)^2}$$

$$M_e = \frac{-\sqrt{2}}{\gamma c_{p_{lim}} \sqrt{1 - M_n^2}} \sqrt{\sqrt{1 + (\gamma c_{p_{lim}} \sqrt{1 - M_n^2})^2} - 1}$$

$$c_{t_n} = c_t \frac{c}{c_n} \frac{1}{\cos^2 \Lambda}$$

$$K_t = \frac{2(1 - M_e^2)}{M_e} \left[\frac{\frac{t_n}{c_n} \left(\frac{r_n}{c_n} \right)^{0.4}}{c_{t_n} \sqrt{1 - M_n^2}} \right]^{0.6}$$

The leading edge thrust is to be reduced by the factor K_t above, which is not allowed to exceed 1.

$$\text{if} \quad K_t > 1, \quad \text{set} \quad K_t = 1$$

In concept, the reduction in leading edge thrust is caused by a vortex separating off the leading edge and moving to some point above the airfoil where it generates the same force, but rotated by $\text{acos} K_t$ as described in figure 7.

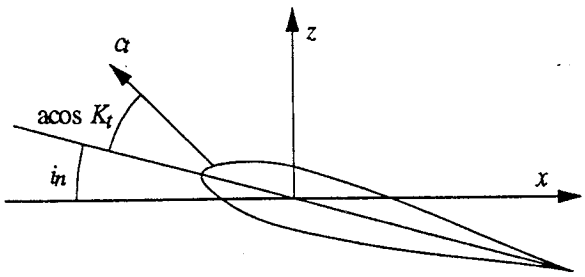

Figure 7: Geometry used in calculating extra lift and drag due to rotation of leading edge thrust.

The effect on lift and drag is calculated, first, by evaluating changes in x and z forces.

$$i = \text{local panel incidence}$$

$$i_n = \text{atan}\left(\frac{\tan i}{\cos \Lambda_{LE}}\right)$$

$$\Delta c_x = -c_t \left[\cos\left(\text{acos} K_t + i_n\right) + \cos i_n\right]$$

$$\Delta c_z = \frac{c_t}{\cos \Lambda_{LE}} \left[\sin\left(\text{acos} K_t + i_n\right) - \sin i_n\right]$$

The local changes in x and z force are accumulated into configuration ΔC_x and ΔC_z. These are then rotated by the angle of attack to obtain ΔC_D and ΔC_L.

References

[1] Smith, S. C., and Kroo, I. M., "A Closer Look at the Induced Drag of Crescent-Shaped Wings," AIAA-90-3063, 1990.

[2] Wakayama, S., and Kroo, I., "A Method for Lifting Surface Design Using Nonlinear Optimization," AIAA-90-3290, 1990.

[3] Mason, W., "Analytic Models for Technology Integration in Aircraft Design", AIAA-90-3262, 1990.

[4] Hutchison, M., Unger, E., Mason, W., Grossman, B., and Haftka, R., "Variable-Complexity Aerodynamic Optimization of an HSCT Wing Using Structural Wing-Weight Equations", AIAA-92-0212, 1992.

[5] Kroo, I., "A General Approach to Multiple Lifting Surface Design and Analysis", AIAA-84-2507, 1984.

[6] Wakayama, S., and Kroo, I., "A Method for Lifting Surface Design Using Nonlinear Optimization", AIAA-90-3290, 1990.

[7] Gallman, J., Kroo, I., and Smith, S., "Design Synthesis and Optimization of Joined-Wing Transports", AIAA-90-3197, 1990.

[8] Grossman, B., Haftka, R., Kao, P., Polen, D., Rais-Rohani, M., and Sobieszczanski-Sobieski, J., "Integrated Aerodynamic-Structural Design of a Transport Wing", *Journal of Aircraft*, Vol. 27, No. 12, 1990, pp. 1050-1056.

[9] Megson, T., *Aircraft Structures for Engineering Students*, Edward Arnold Publishers Ltd., London, 1972.

[10] Gray, W., and Schenk, K., "A Method for Calculating the Subsonic Steady-State Loading on an Airplane with a wing of Arbitrary Planform and Stiffness," NACA TN 3030, 1953.

[11] Technical Report, ASD/XR 72-20, Volume II, Part 2, Appendix G, "Mass Properties Report, Advanced STOL Transport (Medium)", Air Force Contract F33615-72-C-1479, August 1972.

[12] Gallaher, George, and Boughan, Rolla, "A Method of Calculating the Compressive Strength of Z-Stiffened Panels that Develop Local Instability," NACA TN 1482, November 1947.

[13] Furlong, G. Chester, and McHugh, James G., "A Summary and Analysis of the Low Speed Longitudinal Characteristics of Swept Wings at High Reynolds Number," NACA Report 1339, 1957.

[14] Carlson, Harry W., Mack, Robert J., and Barger, Raymond L., "Estimation of Attainable Leading-Edge Thrust for Wings at Subsonic and Supersonic Speeds," NASA TP 1500, 1979.

[15] Callaghan, J. G., "Aerodynamic Prediction for Aircraft at Low Speeds with Mechanical High Lift Devices," AGARD Lecture Series No. 67, von Karman Institute, Brussels, Belgium, May 1974.

[16] Private Communication, Professor R. S. Shevell, Department of Aeronautics and Astronautics, Stanford University.

[17] McCormick, Barnes W., *Aerodynamics of V/STOL Flight*, Academic Press, New York, 1967.

[18] Carlson, Harry W., Mack, Robert J., and Barger Raymond L., "Estimation of Attainable Leading-Edge Thrust for Wings at Subsonic and Supersonic Speeds," NASA TP 1500, 1979.